PR-1 177

MILITARY TECHNICAL COLLEGE

CAIRO - EGYPT

PERFORMANCE OF THE INTEGRAL ROCKET-RAMJETS

A.M.SARHAN*, M.A.EL-SENBAWI**, S.M.ABDEL-GHANY***

ABSTRACT

The work aims at the experimental and theoretical determination of the effect of the air addition on the performance of solid propellant Integral Rocket-Ramjet Motors IRRM's. An experimental investigation was carried out to determine the specific impulse dependence on the air equivalence ratio, using an 80 mm motor with exchangeable external and intermediate nozzles. Air inlets and secondary combustion chamber were kept unchanged. The ducted air by ram effect was simulated in this ground testing by feeding pressurized air into the secondary combustion chamber. The experimental investigation showed that the motor specific impulse was increased by about 85% when the air equivalence ratio was increased from zero to about 0.7.

A simple one dimensional mathematical model of a solid propellant IRRM at steady state is presented. The numerical calculations based on the presented model showed good agreement with the test results.

INTRODUCTION

Only Integral Rocket Ramjet Motors IRRM's, due to their high specific impulse, high speed, continuous thrust and compactness can uniquely meet the urgent needs of the next generation atmospheric missiles, [1]. The October 1973 War 'YOM KIPPUR' convincingly demonstrated the effectiveness of the IRR surface-to-air tactical missiles. The Egyptian air defence inflected sharp losses on the Israeli fighters using the Russian missile SAM-6, which employs the solid propellant IRRM variant.

The main variants of IRRM, as illustrated in Fig.1 are solid propellant IRRM, liquid propellant IRRM, solid propellant IRRM with additional liquid fuel injection into the secondary combustion chamber, and scram-jet rocket motor, where supersonic combustion is allowed in the secondary combustion chamber, [1].

---

* Ph.D., Dep. of Rockets, M.T.C., Cairo.
** Ph.D., Head of Dep. of Rockets, M.T.C., Cairo.
*** Prof., Dep. of Mechanical Power, Ain Shams University, Cairo.

The performance of IRRM compared to that of rockets, turbofans, and turbojets is illustrated in Fig.2 and Fig.3.

According to the purpose of the study, theoretical analysis of IRRM can be tackled by one of the following two approaches:

I. Quasi One Dimensional Analysis

We assume that the angle of the air inlet and the length of the secondary combustion chamber are chosen so that the incompletely burned gases and the ducted air are completely mixed and reacted. For this case, the integral forms of mass, momentum, and energy equations are to be solved together with the equation of state and the laws of the gas mixture. This approach is useful to compute the overall performance of the IRRM.

II. Three-Dimensional Axisymmetric Analysis

Assuming that the turbulent mixing can be mathematically expressed in an accurate mathematical form, the flow field inside the secondary combustion chamber can be fully investigated by solving the differential forms of the equations of mass, momentum, energy, turbulent kinetic energy, turbulence length scale and chemical kinetics of the reactions, together with the equation of state. Due to the fact that the reaction rates of gases are much faster than their mixing rates, [2], the group of equations expressing the reaction rate can be completely ignored without having significant error, [3,4]. That assumption reduces the number of partial differential equations and the stiffness degree of the numerical solution. This approach is useful to find out theoretically the optimum angle of air inlets and the corresponding required combustor length. Besides, the performance of the IRRM can be obtained.

The present work is an experimental and theoretical investigation into the solid propellant IRRM's. The first approach is employed to study the effect of air addition on their performance.

ONE-DIMENSIONAL MATHEMATICAL MODEL

Following Ramanujachary's model, [5], the solid propellant IRRM can be divided into four main parts as shown schematically in Fig.4. These are the air diffuser, the primary combustion chamber, the secondary combustion chamber and the nozzle. The analysis is based on one dimensional flow with the assumption of no heat transfer from the hot gases to the combustor walls.

The Air Diffuser

The IRRM often uses four axisymmetrical conical air diffusers, similar to those of jet engines. The function of the air diffuser

is to decelerate and compress the air flow into the secondary combustion chamber. In ground testing, the air diffusers are replaced by an air feeding system as it will be explained in the experimental part.

The Primary Combustion Chamber

Here, a fuel-rich propellant is burned producing incompletely burned gases. At steady state, assuming small gas velocity, constant chamber volume, negligibly small pressure variation along the propellant grain, isentropic process and frozen flow, the stagnation pressure p_{op} inside this zone has the form

$$p_{op} = \left[K_I \, u_o \, C^* \, \varrho_p \, \mathrm{Exp}[K_T(T_p - T_N)] \right]^{1/(1-n)} \qquad (1)$$

where K_I is the blocking factor defined as the ratio of burning surface to throat area, ϱ_p is the specific mass of the propellant, C^* is the characteristic velocity of the propellant, u_o, K_T and n are propellant constants, and T_p and T_N are the actual and normal propellant temperatures.

The conditions at the throat (which are in the same time the inlet conditions of the secondary combustion chamber) can be given by

$$\dot{m}_{2g} = (p_{og} \, A_{2g}) / C^* \qquad (2)$$

$$T_{2g} = T_{og} \left[2/(k_1+1) \right] \qquad (3)$$

$$p_{2g} = p_{og} \left[2/(k_1+1) \right]^{k_1/(k_1+1)} \qquad (4)$$

$$v_{2g} = \left[2 \, k_1 \, R_1 \, T_{og}/(k_1+1) \right]^{0.5} \qquad (5)$$

where T_{og} is the adiabatic flame temperature of the propellant.

The secondary Combustion Chamber

For simplicity, it is assumed that the ducted air and the incompletely burned gases are subjected successively to processes of mixing, pressure loss, and heat addition at distinct zones.

Mixing zone

In the mixing zone, the incompletely burned gases and the ducted air (both of known parameters p, ϱ, T, v, c_p and R) are mixed together. It is required to compute the gas parameters after complete mixing. The thermodynamic properties of the mixture R_3, $c_{p,3}$ and k_3 are obtained as follows

$$R_3 = R_u / \mu_3 \qquad (6)$$

where $$\mu_3 = 1/(x_a/\mu_a + x_p/\mu_p) \quad (7)$$

and $$x_a = \dot{m}_a/(\dot{m}_{2a} + \dot{m}_{2p}) \quad (8)$$

$$x_p = \dot{m}_p/(\dot{m}_{2a} + \dot{m}_{2p}) \quad (9)$$

$$c_{p,3} = x_a c_{p,2a} + x_p c_{p,2p} \quad (10)$$

$$k_3 = c_{p,3}/(c_{p,3} - R_3) \quad (11)$$

The equations of continuity, momentum and energy are

$$\dot{m}_{2a} + \dot{m}_{2p} = A_3 v_3 p_3/(R_3 T_3) = \dot{m}_3 \quad (12)$$

$$p_{2a} A_{2a}/\cos\beta + \dot{m}_{2a} v_{2a} \cos\beta + p_{2p} A_{2p} + \dot{m}_{2p} v_{2p} = p_3 A_3 + \dot{m}_3 v_3 \quad (13)$$

$$\dot{m}_{2a}(c_{p,2a} T_{2a} + 0.5 v_{2a}^2) + \dot{m}_{2p}(c_{p,2p} T_{2p} + 0.5 v_{2p}^2) = \dot{m}_3(c_{p,3} T_3 + 0.5 v_3^2) \quad (14)$$

These equations are solved simultaneously to get v_3, p_3 and T_3.

Pressure loss zone

Assuming an adiabatic frictional loss (i.e. $T_{o4} = T_{o5}$), the pressure loss is expressed as

$$p_{o3} - p_{o4} = 0.5 K \rho_3 v_3^2 \quad (15)$$

where K is the pressure loss factor which lies within the range $1 < K < 4$, [6]. Eq.15 can be modified to be

$$p_{o4}/p_{o3} = 1-[(K_3/2)(K_3 M_3^2)(1+0.5(k_3-1)M_3^2)k_3/(1-k_3)] \quad (16)$$

From the equations of state and continuity we get

$$p_{o4}/p_{o3} = (M_3/M_4)[(1+0.5(K_3-1)M_4^2)/(1+0.5(K_3-1)M_3^2)]^{(k_3+1)/2(k_3-1)} \quad (17)$$

The values of M_4 and p_{o4} can be obtained by solving Eq.16 and Eq.17 together.

Heat addition zone

The mixture of air and incompletely burned gases flowing from section 4 is ready to burn in the heat addition zone. This mixture has its initial composition as in section 3, and its initial stagnation temperature $T_{o4} = T_{o3}$. So, the equilibrium composition and the values of T_{o5}, R_5 and K_5 can now be calculated using a suitable program of thermochemical calculations [7]. The program is valid for range of α from zero

to the stoichiometric value for the propellant. We proceed for the determination of M_5 and p_{o5} considering a simple constant area heat addition process as follows

From equations of state and continuity we get

$$p_5/p_4 = (M_4/M_5)[(K_4R_5T_{o5})/(K_5R_4T_{o4})]^{0.5} \times$$
$$\times [(1+0.5(K_4-1)M_4^2)/(1+0.5(K_5-1)M_5^2)]^{0.5} \quad (18)$$

In the absence of wall friction loss, the momentum and state equations yield

$$p_5/p_4 = (1+ K_4M_4^2)/(1+ K_5M_5^2) \quad (19)$$

Together with the isentropic flow relation

$$p_{o5} = p_5 (1+0.5(k_5-1) M_5^2)^{k_5/(k_5-1)} \quad (20)$$

the values of M_5, p_5 and p_{o5} can be determined.

The Nozzle

The treatment is based on quasi one-dimensional, isentropic frozen flow through the nozzle. The throat area A^* corresponding to the calculated stagnation pressure and the characteristic velocity C^* (calculated for T_{o5}, R_5 and k_5) is expressed as

$$A^* = C^*m_5/p_{o5} \quad (21)$$

If $A_6 > A^*$, the nozzle will not be choked and no supersonic flow can be attained by this nozzle. If $A_6 < A^*$ the nozzle will be choked but the gas should be accumulated in the secondary chamber for a transient period. The stagnation pressure is thus increased to a new equilibrium stagnation pressure so that the inlet mass flow rate to the secondary chamber should be equal to the mass flow rate of the gases exhausted through the nozzle throat.

$$\dot{m}_6 = \dot{m}_5 \quad (22)$$

The new equilibrium pressure p_{o5} corresponding to the throat area A_6 could be obtained from

$$\dot{m}_6 = p_{o5}A_6/C^* \quad (23)$$

The gas exhaust velocity v_7 is expressed as

$$v_7 = [(2k_5R_5T_{o5}/(k_5-1))(1-(p_7/p_{o5})^{(k_5-1)/k_5})]^{0.5} \quad (24)$$

p_7 is the pressure at the exit section, its value is chosen to be equal to p_a at some altitude for which the maximum global thrust gain is achieved, [8].

The area ratio A_7/A_6 is given by

$$A_7/A_6 = \frac{\Gamma(k_5)}{(p_7/p_{05})^{1/k}[(2k_5/(k_5-1))(1-(p_7/p_{05})^{(k_5-1)/k_5}]^{0.5}} \qquad (25)$$

The thrust of the IRRM can be expressed as

$$F = \eta_n [\dot{m}_6 v_7 - \dot{m}_a v_1 + A_7(p_7 - p_a)] \qquad (26)$$

where η_n is the nozzle efficiency.

The specific impulse i_{sp} is given by

$$i_{sp} = (1/m_p) \int_{t_{ig}}^{t_k} F.dt \qquad (27)$$

EXPERIMENTAL STUDY

A series of tests were carried out using an 80 mm test motor charged with a fuel-rich double-base propellant. The ducted air to the secondary combustion chamber by ram effect was simulated in the tests by feeding a pressurized air into the inlets of the secondary combustion chamber from a pressurized air reservoir. The used propellant had the following data

Summary formula: $C_{23.495}\ H_{31.936}\ O_{34.75}\ N_{9.415}$

Heat of formation: $H_p = -2413.5$ KJ/Kg

Burning rate (in SI units):

$$u = 2.294 \times 10^{-7}\ p^{0.674}\ \mathrm{Exp}[0.00448(T_p - 20)]$$

Simple thermochemical calculation of the propellant combustion, assuming five gas products, gave the following results for the gas products:

- Composition of the gas products given in gram moles per 1 kg of the propellant:
  CO_2: 3.555, CO: 19.939, H_2: 8.268, H_2O: 7.700, N_2: 4.707
- Adiabatic flame temperature = 2175 K
- Molecular mass = 22.6855 Kg
- Gas constant = 366.5 J/Kg K
- Ratio of specific heats = 1.255
- Specific heat at constant pressure = 1800 J/Kg K

Test Rig

Fig.5 shows the general scheme of the test rig which had been used. The basic parts of the test rig are the test motor 1, the thrust test bed 2, the air feeding system 3-8, the pickups 9-13, and the signal conditioning and recording system 14-17.

The test motor was designed to secure the following:

- A specific primary chamber is to be mounted for each length of the propellant grain, namely 10, 15 and 20 cm.
- The critical area of the intermediate nozzle is set for each test so that the working pressure of the primary combustion chamber is kept almost the same.
- The air is introduced to the secondary combustion chamber through four axisymmetric circumferential circular air inlets, with fixed inclination 45^{o} to ensure optimum mixing, [9].
- The length-to-diameter ratio of the secondary combustion chamber is chosen L/d = 8 in order to have complete reaction with minimum pressure losses, [10].
- A set of nozzles of the same expansion ratio, but different critical areas are used to get almost the same working pressure at secondary combustion chamber.

To simulate the ducted air during flight, two 80-liter reservoirs with compressed air at 30 bar were used to supply the secondary combustion chamber with air through four flexible hoses.

The IRRM was mounted on a horizontal type swinging test bed as shown in Fig.6. The thrust and pressure at different positions (air reservoirs, air inlets to the secondary combustor, primary and secondary combustors) were measured by strain-gauge transducers with frequency response up to 20 KHz. The expected measurement error by these transducers is less than 0.5%.

The mass flow of air was computed from the measured parameters of air in the reservoir at the moments of air flow start, motor ignition and burn-out which are described by subscripts "st", "ig" and "k" respectively. These events are marked on the pressure-time records, providing an appropriate means for time determination. Assuming adiabatic process, the mass consumption of air m_a (from ignition to burn-out) is calculated from

$$m_a = (V/R_a T_{st})[p_{ig}(p_{ig}/p_{st})^{(1-k)/k} - p_k(p_k/p_{st})^{(1-k)/k}] \qquad (28)$$

where R_a, k, V are the air gas constant, ratio of specific heats and reservoir volume respectively.

The average mass flow rate $\dot{m}_a$ is computed form

$$\dot{m}_a = m_a/(t_k - t_{ig}) \qquad (29)$$

The difference in the mass flow rate of air from one test to another was kept in narrow limits. A significant control of equivalence ratio α was done by controlling the mass flow rate of the incompletely burned gases flowing to the secondary combustion chamber. The average value of α is expressed as

$$\alpha = m_a/m_p \qquad (30)$$

where m_p is the mass of propellant charge.

Experimental Results

Five main tests were performed to investigate the effect of the air equivalence ratio on the specific impulse of the IRRM. The first four tests were carried out with air addition, while the fifth test was done without air at all to be a basis for the comparison. The numerical values of the tested cases are summarized in Table 1. A sample of the obtained thrust and pressure time traces is presented in Fig.7. The figure shows a constant primary combustor pressure and a linearly varying air reservoir pressure which indicate constant mass flow rates of the incompletely burned gases and the air.

Test data show that the specific impulse is augmented as a result of air injection into the secondary combustion chamber. The specific impulse was increased from 1404 to 2600 m/S with an 85% increase, when the equivalence ratio was increased from zero to 0.686. Further increase may be expected as far as complete combustion has not yet been attained. The low secondary combustion chamber pressure, (resulting from low possible attained diffuser pressure) leads to limited expansion ratio through the nozzle. Consequently, IRRM's are more suitable for the flight at high altitudes where greater expansion ratios can be reached.

Table 1. Test data

Parameter	1	2	3	4	5
Mass of propellant, Kg	0.4	0.4	0.585	0.785	0.600
Intermediate nozzle throat diameter ,mm	11.5	11.5	13.0	14.5	11.5
Main nozzle throat diameter, mm	25.5	24.5	25.5	30.0	24.5
Area Ratio A_e/A_t	4.15	4.16	4.15	4.0	4.16
Air inlet average pressure, bar	12.2	10.2	10.5	9.85	—
Air reservoir pressure at ignition, bar	15.6	15.6	15.6	13.0	—
Air reservoir pressure at burn-out, bar	14.0	14.0	14.4	12.0	—
Mass of inlet air, Kg	0.276	0.137	0.102	0.090	0.000
Air equivalence ratio,	0.686	0.343	0.174	0.114	0.000
Primary chamber average pressure, bar	58.8	58.8	45.0	54.0	78.8
Secondary chamber average pressure, bar	9.0	8.7	9.0	7.0	17.0
Average thrust, N	866.6	650.0	668.6	980.7	773.5
Time of function, S	1.200	1.20	1.400	1.240	1.090
Total impulse, NS	1039.9	780	936.0	1215	842.5
Specific impulse, N S/Kg	2600	1950	1600	1548	1404

COMPUTED RESULTS

Numerical computations using the presented mathematical model were carried out for the tested cases. These results are summarized in table 2.

Table 2. Results of Theoretical calculations

Test No.	α	T_{o5} K	K_5	R_5 J/Kg.K	p_{o5} bar	v_7 m/s	F N	i_{sp} Ns/Kg
Test 1	0.687	2550	1.235	323.0	12.86	1950	815.5	2650.0
Test 2	0.3432	2350	1.245	331.3	11.76	1941	625.8	2033.7
Test 3	0.1742	2275	1.250	346.5	12.64	1938	703.4	1803.0
Test 4	0.1144	2200	1.253	352.6	12.56	1920	1018.8	1726.8
Test 5	0.0	2175	1.255	366.5	17.18	1957	919.5	1672.9

Comparison between the theoretical and experimental values of the specific impulse as function of the air equivalence ratio is presented in Fig.8. It can be noticed that the difference between the theoretical and experimental results is relatively great for small values of α and it gradually gets smaller as the values of α increase. This can be explained by the fact that the mathematical model assumes no heat transfer through the walls to the surroundings, while the thick-walled test motor absorbs a considerable amount of heat. This amount can be neglected relative to the great liberated heat for higher values of α. However, the heat absorbed by the walls tends to be comparable with the low heat liberated for small values of α. Taking into consideration that real motors normally operate at higher equivalence ratios, and that they usually have thinner walls compared to test motors, one can come to the conclusion that the presented model provides an efficient tool for practical application.

Theoretical investigation was carried out for the dependence of specific impulse and adiabatic flame temperature in the secondary combustor for the range of α from zero to the stoichiometric value $\alpha = 1.8$. Results are presented in Fig.9 and Fig.10 respectively. The specific impulse showed a monotonic increase with the increase of α in the full investigated range. On the other hand, the temperature increased steadily with α, up to $\alpha = 0.7$ then it showed approximately constant value. This can be explained by the dilution effect of the nitrogen content in air. Such behavior is favorable in real application from the point of view of thermal effects on combustor walls.

CONCLUSION

The specific impulse is augmented as a result of the air injection into the secondary combustor. The specific impulse showed an increase of 85% when the air equivalence ratio was increased from zero to 0.7. Computed values for the test cases showed good agreeament with the experimental results, in particular, for higher values of α. Further theoretical investigations for the full range of α from zero to 1.8 (which is the stoichiometric equivalence ratio for the used propellant) showed that the specific impulse increases monotonically with α. On the other hand, the adiabatic flame temperature of the reaction in the secondary combustor showed monotonic increase with the increase of α from zero up to 0.7 then it kept an almost constant value. It is recommended to design IRRM's with high α.

NOMENCLATURE

A	Area
C^*	Characteristic velocity
C_p	Molar specific heat at constant pressure
C_v	Molar specific heat at constant volume
c_p	Specific heat at constant pressure
c_v	Specific heat at constant volume
d	Diameter
H	Enthalpy
h	Specific enthalpy
I_{sp}	Specific impulse
K	Pressure loss factor, $1 < K < 4$
k_I	Blocking factor
k	Ratio of specific heats
M	Mach number
m	Mass
$\dot{m}$	Mass flow rate
n	Pressure exponent of the propellant
p	Pressure
R	Gas constant
R_u	Universal gas constant
T	Temperature
T_N	Normal temperature
t	Time
u	Propellant burning rate
u_o	Constant of burning rate
V	Volume of air reservoir
v	Velocity
x	Mass fraction
α	Air equivalence ratio
β	Angle of air inlet
$\Gamma(k)$	Function of the ratio of specific heats
η_n	Nozzle pressure loss
μ	Molecular mass
ϱ	Specific mass

Subscripts

2	Entry to the mixing zone
3	Entry to the pressure loss zone
4	Entry to the heat addition zone
5	Entry to the nozzle
6	Entry to the nozzle critical area
7	Entry to the nozzle exit area
a	Air
g	Incompletely burned gases
ig	at ignition
k	at end of function
o	Stagnation condition
p	Propellant
st	at starting

REFERENCES

1. Thomas, N. Arthur and Thomas, JR, " New Generation Ramjet, A Promising Future", Astronautics and Aeronautics, Vol.18, Jan. 1980, pp 36-41, 71.
2. Ramos, J.I., "The Numerical Solution of Non-Premixed Reactive Flows in a Swirl Combustor Model", Updated and Enlarged Version of the International Conference of Numerical Methods in Non-Linear Problems, Barcelona Spain, April 9-13, 1984.
3. Ghoniem, F. Ahmed, "Computational Methods in Turbulent Reacting Flow", Lectures in Applied Mathematics, Vol.24, 1986, pp 199-239.
4. Arbib, H. A., Goldman, Y., Greenberg, J.B. and Timnat, Y.M., Numerical Model of High Intensity Confined Hydrocarbon Combustion", Combustion and Flame, Vol. 38 1980, pp 259-270.
5. Ramanujachary, V. et al., "Performance Analysis of Primary and Secondary System of a Rocket-Ramjet Engine Burning Fuel-Rich Metallized Propellant", Fifth International Symposium on Airbreathing Engines, Bangalore, India, (1981).
6. Hill, G. and Peterson, R., "Mechanics and Thermodynamics of Propulsion", Addison Wesley, Massachusetts, 1965, p 220.
7. Sarhan, A. "An Experimental Investigation into the Performance of an Airbreathing Rocket Motor", M.Sc. Thesis, Military Technical college, Egypt, (1984).
8. Barrere, M. "Rocket Propulsion", Elsevier Publishing Company, (1960).
9. Greenberg, J.B. and Timnant, Y.M., "Sudden Expansion Injection for Ram-Rockets", Fifth International Symposium on Airbreathing Engines. Bangalore, India, (1981).
10. Chen Da-ming et al.,"Preliminary Experimental Study of in the Solid Propellant Rocket-Ramjet", Fifth International Symposium on Airbreathing Engines, Bangalore, India, (1981).

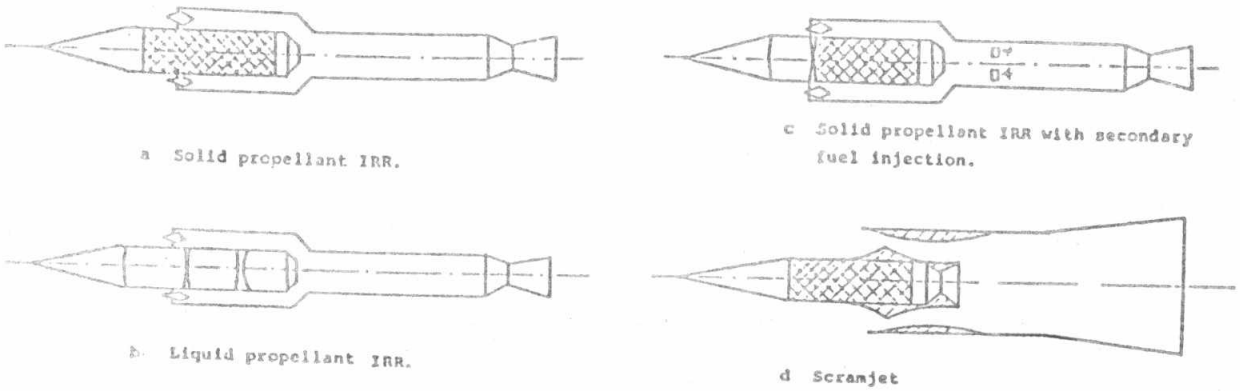

Fig.1 Variants of integral rocket ramjets

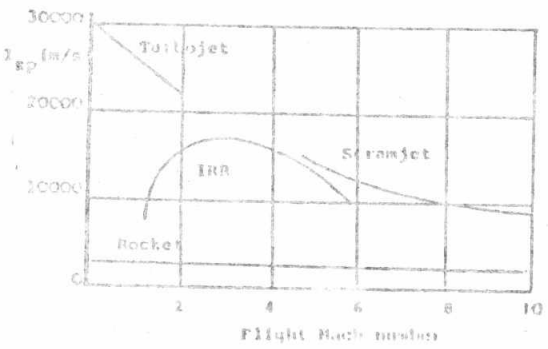

Fig.2 Specific impulse/speed

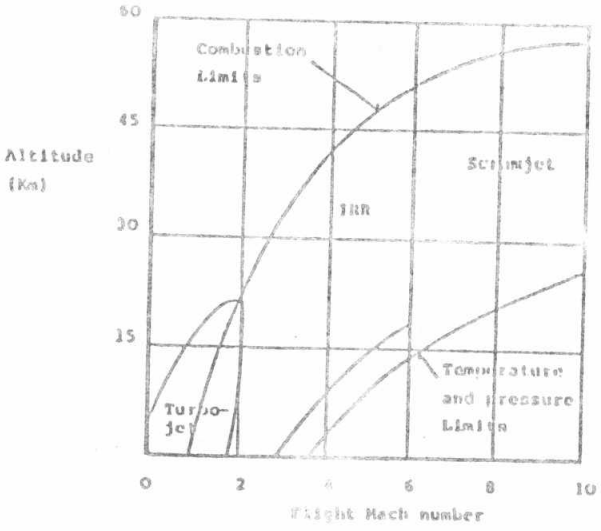

Fig.3 Speed/altitude

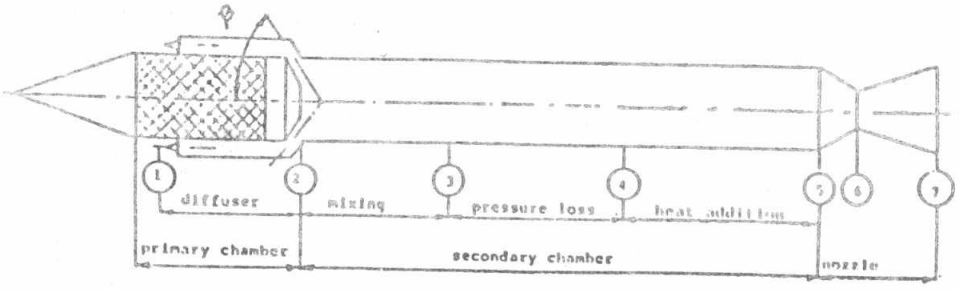

Fig.4 Schematic sketch of solid propellant IRRM

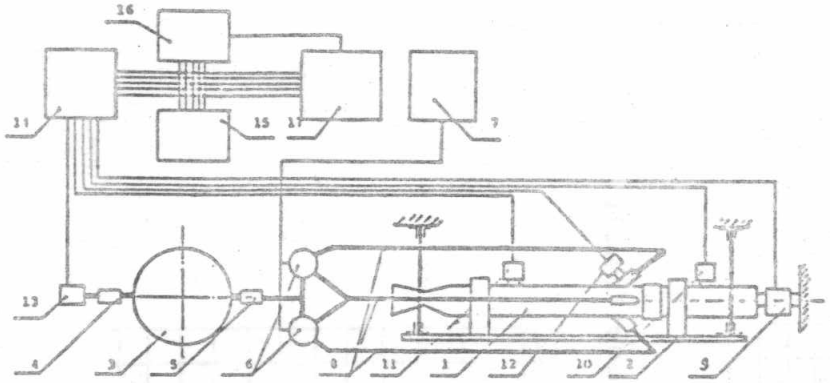

Fig.5 Schemtic diagram of the test rig

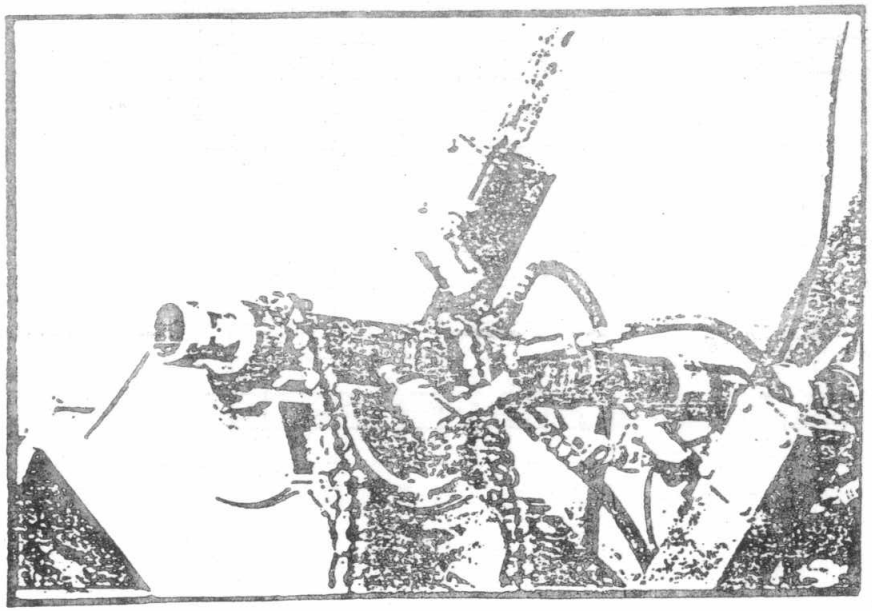

Fig.6 The IRR test motor mounted on its test bed

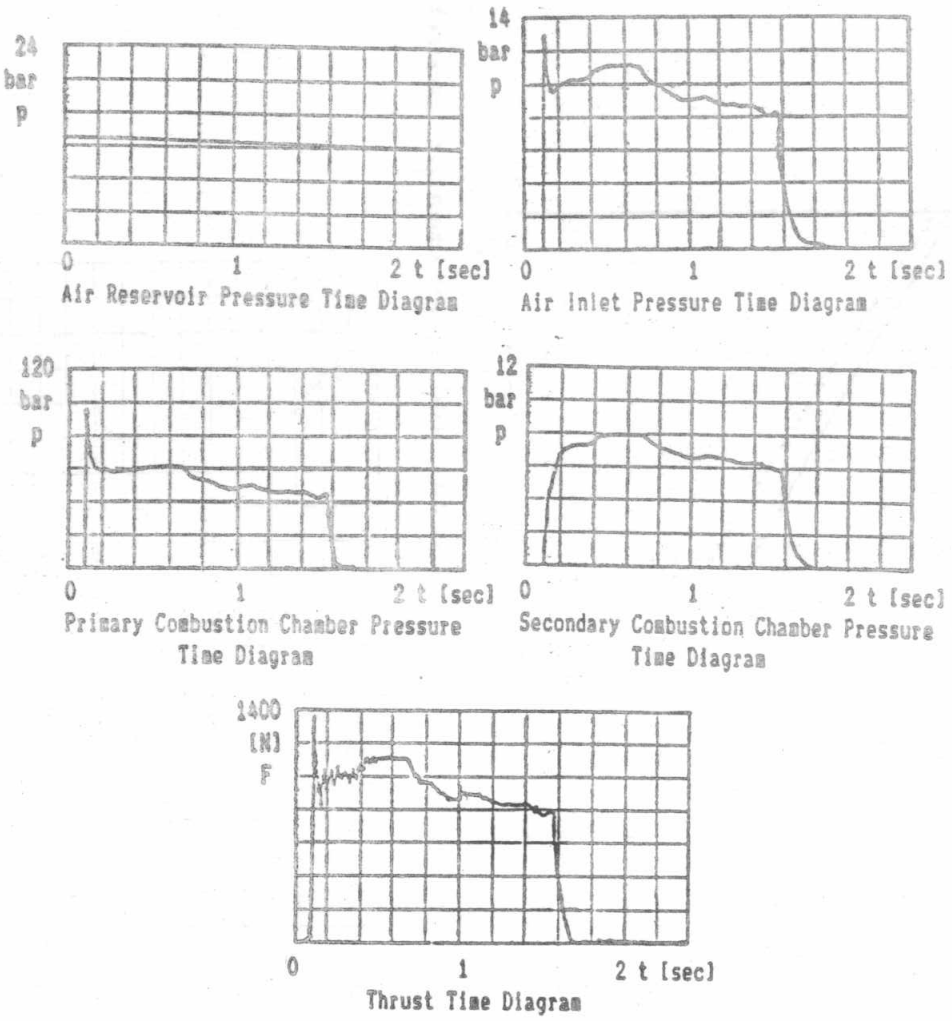

Fig.7 A sample of recorded test data

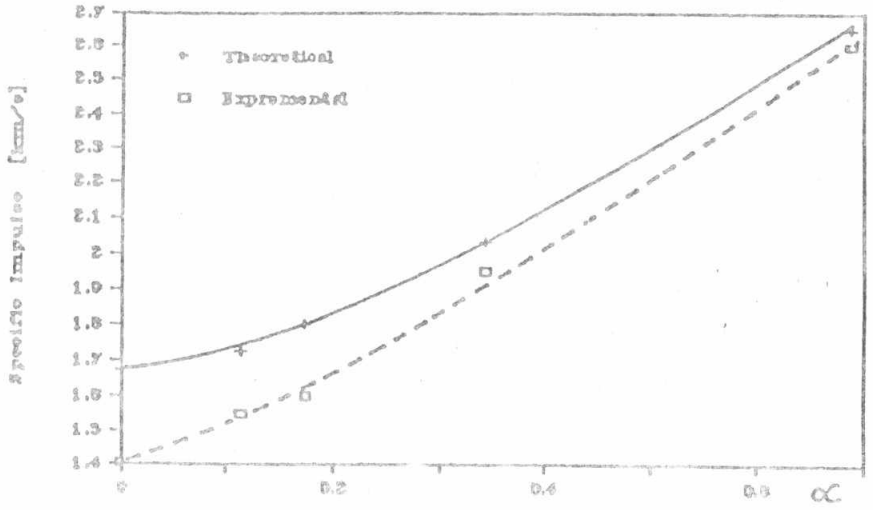

Fig.8 Comparison between theoretical and experimental results

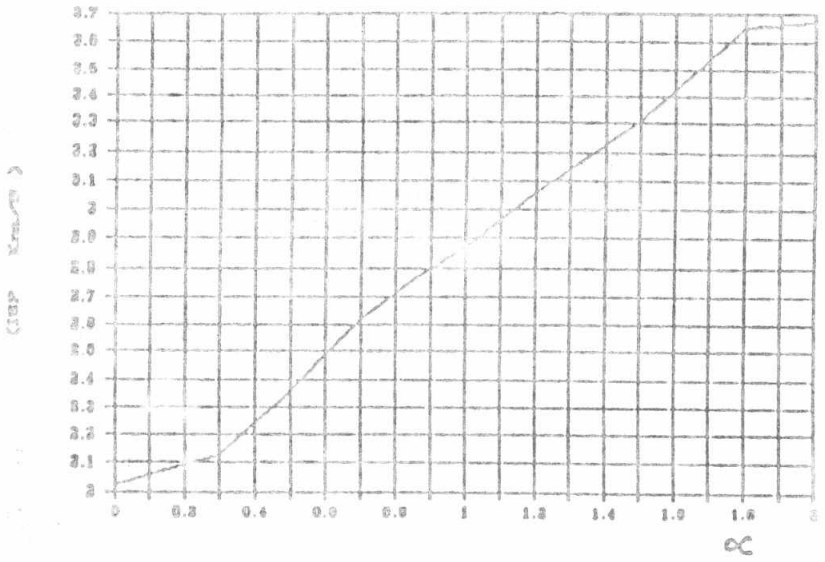

Fig.9 Specific impulse vs. air equivalence ratio

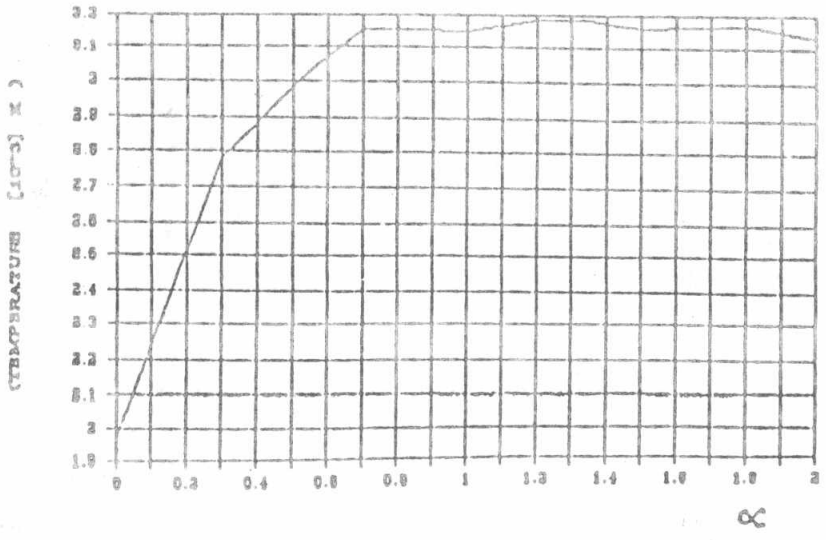

Fig.10 Adiabatic flame temperature vs. air equivalence ratio